Advances in Environmental Technology 4 (2017) 205-216

Advances in Environmental Technology

journal homepage: http://aet.irost.ir

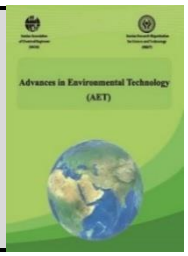

Preparation, characterization and photocatalytic degradation of methylene blue by Fe^{3+} doped TiO_2 supported on natural zeolite using response surface methodology

Hadieh Taghvaei, Mehrdad Farhadian*, Nila Davari, Samira Maazi

Department of Chemical Engineering, Faculty of Engineering, University of Isfahan, Isfahan, Iran

ARTICLE INFO

Article history:
Received 11 September 2017
Received in revised form
5 May 2018
Accepted 21 May 2018

Keywords:
Methylene blue
Photocatalyst
TiO_2/Fe_2O_3
Natural Zeolite
Response Surface Methodology

ABSTRACT

The photocatalytic degradation of methylene blue was investigated with TiO_2 and Fe_2O_3 nanoparticles supported on natural zeolite. The synthesized photocatalyst was characterized by XRD, XRF, FT-IR, EDX, FE-SEM, and BET analyses. The results of XRD, FT-IR, and EDX confirmed the successful loading of Fe^{3+} doped TiO_2 nanoparticles on natural zeolite. Further, the FE-SEM results confirmed the deposition of TiO_2/Fe_2O_3 on the zeolite, with the approximate particle size being 52.3 nm. According to the XRF results, the synthesized nanoparticles had Fe^{3+}/TiO_2 molar ratios of 0.06 in the synthesized photocatalyst. Based on BET analysis, the surface area of TiO_2/Fe^{3+}/natural zeolite was about 112.69 m^2/g. The effects of operational factors such as pH (6-10), dye concentration (25-75 mg/L) and H_2O_2 concentration (10-40 mg/L) were considered and optimized via response surface methodology utilizing Box-Behnken design. The optimization results indicated that the maximum percentage of degradation was achieved at a dye concentration of 25 mg/L, initial pH of 10, and H_2O_2 concentration of 40 mg/L with a 90 min irradiation time and a 1 g/l photocatalyst concentration. The dye degradation efficiency reached 92% under this optimum condition.

1. Introduction

With the development of dye manufacturing industries, their wastewater has become one of the main sources of water pollution [1]. Currently, the vast majority of synthetic dyes with aromatic compounds are potentially toxic and difficult to degrade. Therefore, the discharge of their wastewater can indirectly affect human health through the food chain as well as causing serious problems for to the environment [2]. Methylene blue (MB) is amongst the most commonly used dyes in textile industries and consists of various aromatic amine groups, which are extremely carcinogenic and mutagenic. Therefore, the development of new treatment methods before its release into the environment has always been an important issue in the present day context [3]. In recent years, advanced oxidation processes (AOPs) have been used as a substitute for treatment [4]. In these processes, unstable radicals, especially free hydroxyl radicals, are used for degrading pollutants via conversion to harmless minerals such as carbon dioxide, water, and mineral salts [5]. Among all of the AOPs methods, photocatalytic degradation has shown to be an effective means for degrading organic pollutions. TiO_2 is one of the best options for pollutant degradation, thanks to its good catalytic activity, high chemical and optical stability, hard solubility, nontoxic, no need for high energy, high efficiency, no pollution production, and low cost [6,7]. In most studies, particulate TiO_2 photocatalysts have been used, which are easy to aggregate in aqueous solutions but difficult to recycle and re-collected after use. To solve this problem, many researchers have suggested various methods to stabilize TiO_2 on materials such as ceramic, glass beads fiberglass, activated carbon, stainless steel, zeolite, etc. [8]. Meanwhile, the application of natural zeolite has attracted special attention in recent years due to its extremely low price and relative abundance. TiO_2 deposition on zeolite improves the photocatalytic activity of the zeolite along with its adsorption properties. Further, it

*Corresponding author. Tel: +98 313 7934532
E-mail address: m.farhadian@eng.ui.ac.ir
DOI: 10.22104/AET.2018.2462.1124

has been found that the absorption of visible light can be achieved with the composites of TiO_2 and Fe_2O_3, as a photocatalyst can respond to visible light due to the narrow band-gap of Fe_2O_3 [9]. Many researchers have synthesized TiO_2 photocatalysts and investigated their photocatalytic activity by degrading various organic pollutants such as auramine [9], dye [10], and aryl halides in solution. In addition, many parameters affect photo-degradation such as initial pH, photocatalyst dosage, dye concentration, H_2O_2 concentration, and irradiation time. Niu et al. investigated the effect of the dosage of hydrogen peroxide and dye concentration on the photocatalytic degradation of methylene orange by titanium dioxide-decatungstate nanocomposite [11]. The experimental results revealed that the degradation rate of MO decreases with an increase of initial dye concentration and the addition of hydrogen peroxide, with the concentration within the range of 2.5–20 mM and evidently improving the decolorization rate [11]. Song et al. investigated the effect of graphene-TiO_2 nanotubes (photocatalyst) loading, $KBrO_3$ initial concentration, and amoxicillin (pollution) concentration on photocatalytic activity [12]. Table 1 provides some of the previous reports, representing the effective and measured parameters on the degradation of MB with different catalysts and conditions. As can be seen, TiO_2/Fe^{3+}/natural zeolite has not been used before and all of the results have been measured one at a time. Accordingly, researchers have not evaluated the effect of all of the parameters simultaneously and in most papers, the effects of pH and H_2O_2 were ignored. Furthermore, the concentration of dye applied in the published research was low (lower 30 mg/L), while this paper evaluated the effectiveness of the photocatalyst at a high dye concentration.

Table 1. Recently reported catalytic processes for MB removal with different catalysts

Catalyst	Conditions			References
	Amount of catalyst (mg)	MB concentration (mg/l)	Time (min)	
Ag-ligand modified tungstovandates	10, 20, 30, 40	5	5, 10, 15, 20, 30, 40	[13]
poly(EPE)/f-MWCNT	2	0.2	30, 60, 90, 120, 150, 180	[14]
TiO_2-Mn oxide	25	10	120	[15]
MnOx/WO_3 nanoparticles	10	10	0-120	[16]
Layered manganese oxide	10	30	100	[17]

In this study, the combinational photocatalyst of TiO_2/Fe^{3+} based on natural zeolite was initially synthesized. For the characterization, XRD, XRF, FT-IR, EDX, FE-SEM, and BET analyses were performed on the photocatalyst. The literature review revealed that for the first time, the application of the synthesized photocatalyst on the degradation of MB was examined by analyzing the effect of initial pH, dye concentration, and H_2O_2 concentration on the photo-degradation through response surface methodology (RSM) utilizing Box-Behnken design (BBD).

2. Materials and methods

2.1. Materials

The main precursors used for the preparation of the photocatalyst were $TiCl_4$ (CAS#812382) and $FeCl_3$ (CAS#803945). HCl (CAS#113136), NaOH (CAS#1310732), and H_2O_2 (CAS#822287) with purities of 37, 95, and 30 %, respectively, were used in the experiments. All chemicals were purchased from Merck. The natural zeolite was prepared from the mines of Semnan, Iran. Additionally, the textile dye used in the experiments was MB; it was supplied by Gol Nesar Textile Company, Iran. The characteristics of the mentioned dye are presented in Table 2. When the dye degrades, the following reactions take place [18].

According to reaction below, oxidation of the water absorbed onto the surface of the photocatalyst leads to the production of a hydroxyl radical:

$$H_2O \rightarrow H^+ + {}^\circ OH \quad (1)$$

Then the reduction and oxidation reactions occur as described below:

$$OH^- + h^+ \rightarrow {}^\circ OH \quad (2)$$

$$O_2 + e^- \rightarrow O_2^- \quad (3)$$

Finally resulting in the degradation of MB:

$$MB + {}^\circ OH \rightarrow CO_2 + H_2O + NH_4^+ + NO_3^- + SO_4^{2-} + Cl^- \quad (4)$$

Table 2. Characteristics of the dye

Dye name	Chemical formula	Dye structure	Molecular weight (g/mol)	λ_{max} (nm)
MB	$C_{16}H_{18}ClN_3S$	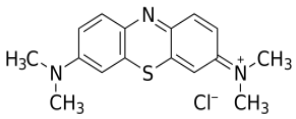	319.85	660

2.2. Photocatalyst preparation

The applied photocatalyst (TiO_2/Fe^{3+}/natural zeolite) was prepared through the co-precipitation method [19]. In order to synthesize the photocatalyst, a specific amount of the prepared natural zeolite powder was mixed with distilled water and the solution was heated to reach a temperature of 70 ºC. Then, specific amounts of $TiCl_4$ and $FeCl_3$ solutions were added into the solution, where the TiO_2 proportion was theoretically calculated to reach 50 wt% of the total photocatalyst. After that, the solution was stirred and washed with deionized water several times; then, it was dryedin the oven. Finally, the powders were calcinated and the desired photocatalyst was synthesized. The details have already been reported in our previous research [8].

2.3. Reactor configuration

The reactor designed for the experiments of photocatalytic dye degradation was a 250-ml batch reactor with a water circulation jacket around it and a 6 W ultraviolet (UV) lamp (with 254 nm wavelength) located in the middle. The reactor was placed on a heater-stirrer in order to generate a magnetic field and continuously spin. The little magnet inside the dye solution kept the photocatalyst particles suspended throughout the entire experiment. The temperature of the experiment was monitored by a digital thermometer placed on the top of the reactor so as to remain constant at room temperature. The reactor apparatus is shown in Figure 1.

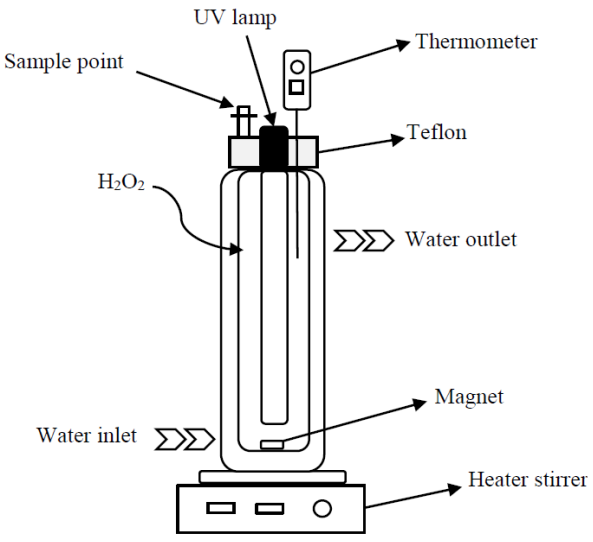

Fig. 1. Schematic view of the photocatalytic reactor

2.4. Characterization

To characterize the synthesized photocatalyst, XRF, XRD and FT-IR analyses were conducted using an x-ray fluorescence device (S4-Pioneer, Bruker, Germany), an x-ray diffraction device (D-8 Advance, Bruker, Germany) and a Fourier transform infrared spectrometer FT-IR-6300 (Jasco, Japan), respectively. The morphology of the synthesized photocatalyst was examined by a scanning electron microscopy device (SEM, XL series, Phillips XL30) equipped with EDX analysis (AIS2300C, SERON Technology) and an FE-SEM device (S-4160, Hitachi Japan). Also, the Brunauer-Emmett-Teller analysis was performed in order to measure pore volume and surface area of the samples by means of N_2 adsorption at 77K (Belsorp mini, Japan).

2.5. Design of experiment (DOE)

In this study, the optimization of experimental conditions for the degradation of MB was conducted via RSM using BBD. The study was conducted using Design Expert software, version 7. Three independent parameters, namely (i) initial pH, (ii) dye concentration, and (iii) H_2O_2 concentration, were altered for optimizing the photodegradation of MB. The experimental design was constructed using three coded values for each variable, (-1), (0), and (+1), which were equally spaced as shown in Table 3. The model was expressed by a second order polynomial function defined by Eq. 5.

$$Y(\%) = \beta_0 + \sum \beta_i X_i + \sum \beta_{ii} X^2 + \sum \beta_{ij} X_i X_j \quad (5)$$

Table 3. Factors and their levels for design of experiments

Factor	Levels		
	-1	0	+1
Initial pH	6	8	10
Dye concentration (mg/l)	25	50	75
H_2O_2 concentration (mg/l)	10	20	40

2.6. Photocatalytic Tests

For each experiment, a solution of the dye with the desired concentration was prepared, and after adjusting the pH value, it was transferred into the reactor chamber along with a constant dosage of the photocatalyst (1 g/L) and desired H_2O_2 concentration. The pH of the solutions was adjusted on desired values using HCl and NaOH diluted

solutions with the help of a Denver UB-10 pH meter. The temperature of the reaction was monitored by a circulating cooling water jacket, keeping it constant at room temperature (25±1 °C). Once the reaction period (90 min) was over, the resulting solution was analyzed by the UV-Vis method with a spectrophotometer device V-570 (Jasco, Japan). In order to monitor the dye concentration, samples of the solution were taken out of the reactor after the reaction time. Then, the photocatalyst particles were filtered and separated after a 10-min centrifugation process at 5000 rpm in a UniCen-Herolab Centrifuge. Afterwards, the solution was analyzed by the UV-Vis method at the maximum wavelength (λ_{max} = 660 nm) for MB, and the dye concentration was calculated using its calibration curve. The efficiency of MB can be calculated by the following equation:

$$\text{Efficiency}(\%) = \frac{C_0 - C_e}{C_0} \times 100 \quad (6)$$

where C_0 and C_e (mg/l) are the initial and final dye concentrations, respectively. Moreover, the actual textile effluents were analyzed for chemical oxygen demand (COD) in accordance with standard method laboratory procedure. After determining the initial and final COD, the efficiency was determined via Eq. 6.

3. Results and discussion

3.1. Characterization of the synthesized photocatalyst

3.1.1. XRD analysis

XRD analysis was performed to detect the TiO_2 nanoparticles based on the natural zeolite and to ensure the preservation of the zeolite structure. The XRD patterns of natural zeolite and the synthesized photocatalyst are presented in Figure 2. According to Figure 2, the XRD pattern of the natural zeolite at 2θ=22.31° and 26.6° has a major peak, which is similar to that reported in a previous study [20]. Furthermore, the main peak positions of natural zeolite (clinoptilolite) have remained almost constant, indicating the structure of clinoptilolite as the support of the photocatalyst. In the XRD pattern of the synthesized photocatalyst, 2θ=25.8°, 48.2°, and 54.4° relating to the anathase TiO_2 can be observed, which is in line with the peaks stated in the literature [19]. The peak of Fe^{3+} is not clearly detectable with XRD analysis because of the low iron content [19]. In XRF, EDX, and FT-IR analyses, the presence of iron has been confirmed.

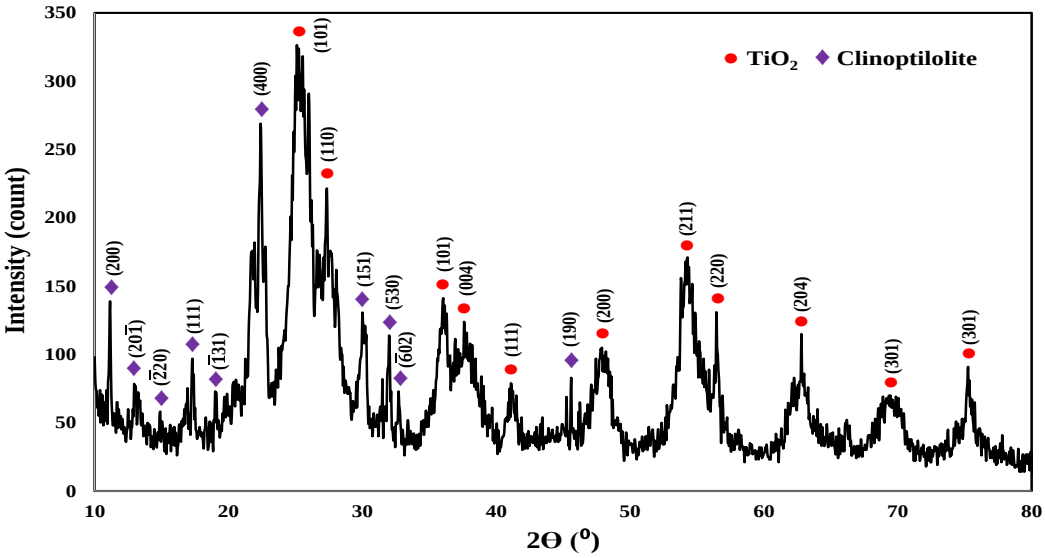

Fig. 2. XRD analysis of natural zeolite and the synthesized photocatalyst

3.1.2. XRF analysis

To determine the composition of different elements in the structure of the synthesized photocatalyst, XRF analysis was performed (Table 4). The results indicated that the photocatalyst contained 55 wt. % of TiO_2 and around 3 wt. % of iron was synthesized. Also, the Fe^{3+} to TiO_2 molar ratio was equal to 0.06 in the synthesized photocatalyst.

Table 4. XRF analysis of natural zeolite and the synthesized photocatalyst

Compound	Natural zeolite concentration (wt. %)	Photocatalyst concentration (wt. %)
SiO_2	79.80	32.85
Al_2O_3	11.53	4.95
CaO	1.91	0.27
Na_2O	1.93	0.88
K_2O	1.80	0.67
Fe_2O_3	1.46	3.50
MgO	1.04	0.43
TiO_2	0.19	55.50
SO_3	0.12	0.14
SrO	0.18	0.03
CuO	0.04	0.03
Cl	-	0.75
Total	100	100

3.1.3. FT-IR Analysis

In the FT-IR spectrum (Figure 3), the peaks associated with zeolite have been repeated in the synthesized photocatalyst. Three additional peaks can be observed at the wave number of about 560, 1100, and 3500 in the synthesized photocatalyst, which are related to that stretching vibration of the Fe-O functional group of iron oxide nanoparticles [21], Ti-O functional group of titanium oxide nanoparticles [22], and superficial hydroxyl group (O-H) of TiO_2 and Fe_2O_3 particles, respectively.

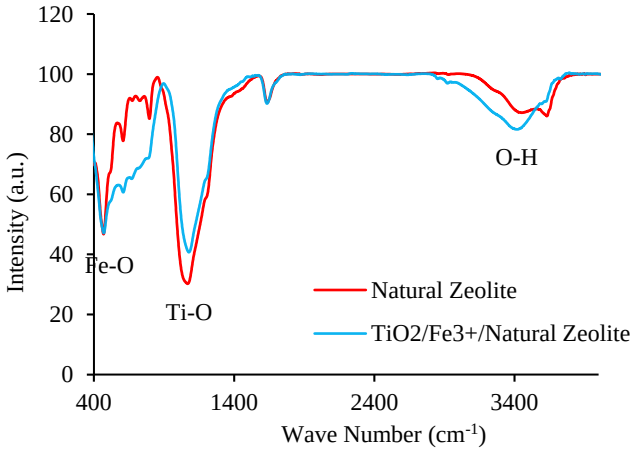

Fig. 3. FT-IR spectrum of natural zeolite and TiO_2/Fe^{3+} photocatalyst deposited on zeolite

3.1.4. EDX and FE-SEM analysis

The EDX spectrum for natural zeolite and the synthesized photocatalyst is demonstrated in Figure 4. The results confirm the loading of Ti and Fe (related to photocatalyst) as well as Al and Si (related to natural zeolite). Moreover, in the EDX of natural zeolite (Figure 4a), Ti is not detected, while Ti in the TiO_2/Fe^{3+}/ natural zeolite EDX (Figure. 4b) is detected.

The FE-SEM image of natural zeolite and the synthesized photocatalyst is presented in Figure. 5 with a scale of 375 nm. Figure 5a indicates no stabilization of nanoparticles on natural zeolite. In Figure. 5b, the surface of the synthesized photocatalyst is observed. The approximate size of the synthesized photocatalyst is 52.3 nm.

The diameter of the synthesized photocatalyst particles was measured by Image J 1.44 p software (Figure 6). According to Figure 6, the size distribution ranged between 1 and 100 nm. Around 20% of photocatalyst particles had a diameter of 10-20 nm, and the lowest share was related to photocatalyst particles with a diameter of 80-90 nm.

3.1.5. BET analysis

The BET analysis was performed for investigating the surface area and pore volume on natural zeolite and the synthesized photocatalyst (Table 5). As can be seen, natural zeolite has a greater surface area and pore volume in comparison with TiO_2/Fe^{3+}/natural zeolite. Indeed, it seems that the successful deposition of TiO_2/Fe^{3+} on the surface and inside natural zeolite pores has reduced the surface area and pore volume.

Table 5. The BET analysis for natural zeolite and the synthesized photocatalyst

Compound	**BET surface area (m^2/g)**	**Pore volume (cm^3/g)**
Natural Zeolite	376.54	0.420
TiO_2/Fe^{3+}/natural	112.69	0.104

3.2. Results of photocatalytic experiments on MB degradation

A total of 15 experiments were performed in random order as required by the design. Further, the photocatalytic experiments were carried out on MB dye at different initial pH values (6-10), dye concentrations (25-75) mg/l, and H_2O_2 concentrations (10-40) mg/L. The photocatalyst concentration and irradiation time were constant and equal to 1 g/L and 90 min, respectively, across all of the experiments. The results are shown in Table 6. According to Table 6, the optimum conditions for the highest efficiency were pH (10), dye concentration (25 mg/L), and H_2O_2 concentration (20 mg/L), with the efficiency reaching 91%.

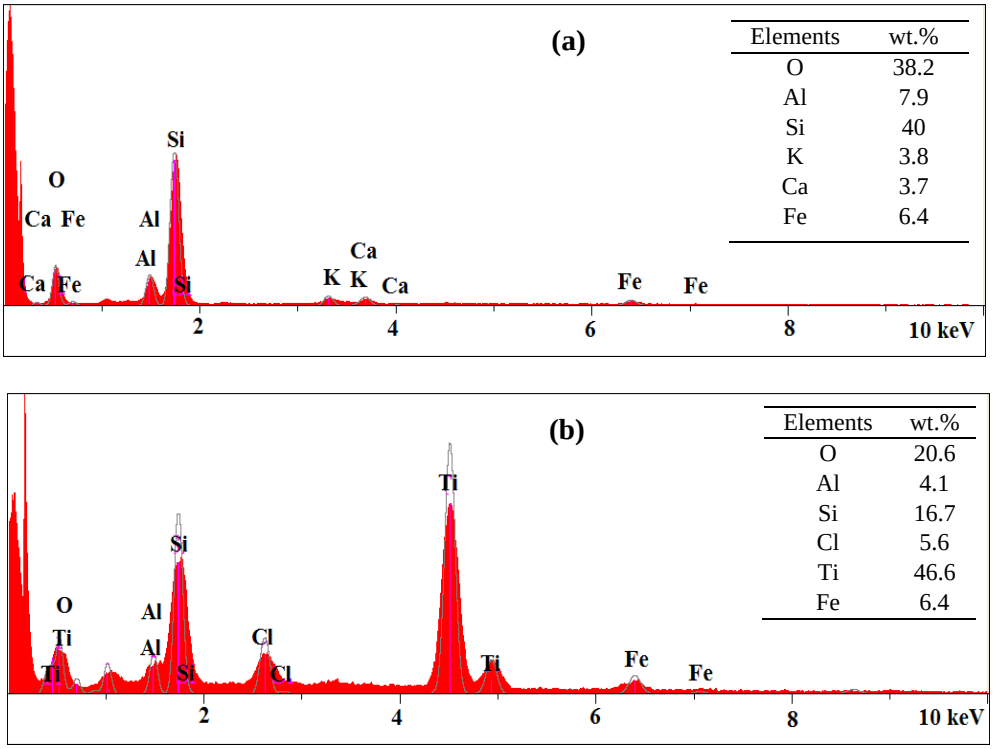

Elements	wt.%
O	38.2
Al	7.9
Si	40
K	3.8
Ca	3.7
Fe	6.4

Elements	wt.%
O	20.6
Al	4.1
Si	16.7
Cl	5.6
Ti	46.6
Fe	6.4

Fig. 4. EDX spectrum for (a) natural zeolite and (b) the synthesized photocatalyst

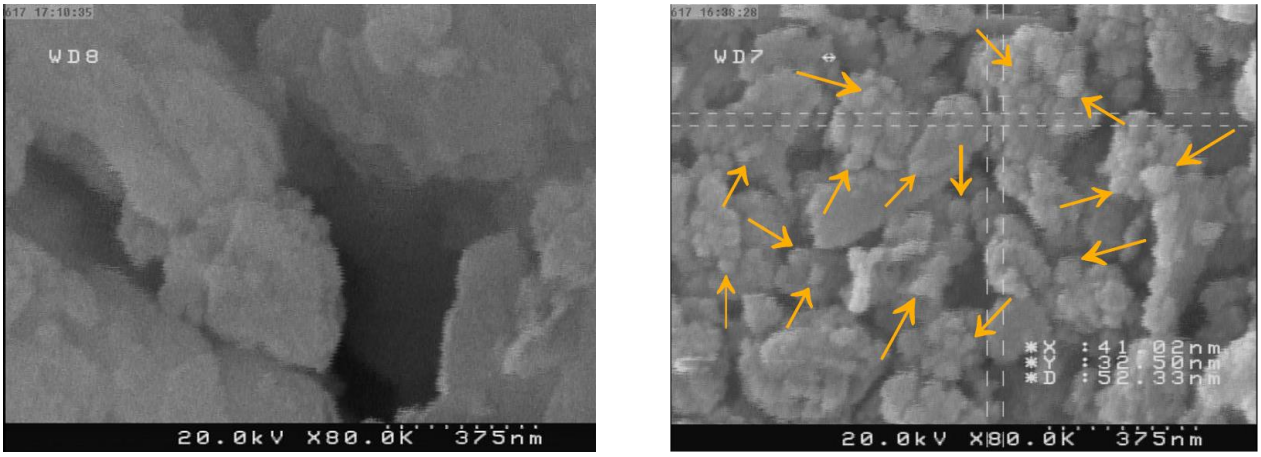

Fig. 5. FE-SEM image for (a) natural zeolite and (b) the synthesized photocatalyst

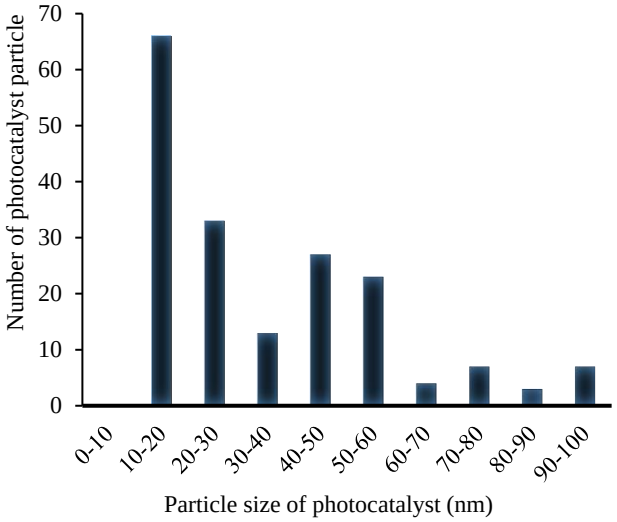

Fig. 6. The particle size distribution of the synthesized photocatalyst

3.2.1. Optimization of MB degradation conditions using the RSM approach

For RSM involving BBD, a total of 15 experiments were conducted for three factors at three levels. The Model F-value of 7.36 implies that the model is significant. There is only a 2.03% chance that a "Model F-Value" this large could occur due to noise. The values of "Prob > F" that are less than 0.0500 indicate that the model terms are significant. The adequacy of the proposed model was then revealed using the diagnostic test provided by analysis of variance (ANOVA). Regression analysis was used to obtain the fitted quadratic polynomial equation. Its equation was then used to develop the response surfaces and contour plots. Therefore, according to Table 7 (ANOVA table), two factors were found to be significant, namely dye concentration and initial pH. Meanwhile, a higher F-value indicates that a factor is more important than the others and has the most impact on the response. Therefore, the mentioned factors were respectively the most effective parameters in the experiments based on their F-values.

Table 6. RSM results for MB

Run number	pH (± 0.01)	Dye concentration (mg/l)	H_2O_2 concentration (mg/l)	Efficiency (%)
1	6	75 ± 0.5	20 ± 0.2	31.2 ± 0.2
2	10	75 ± 0.5	20 ± 0.2	52.4 ± 0.2
3	8	50 ± 0.4	20 ± 0.2	77.1 ± 0.3
4	10	75 ± 0.5	40 ± 0.5	29.3 ± 0.1
5	10	25 ± 0.2	40 ± 0.5	92.5 ± 0.5
6	8	75 ± 0.5	40 ± 0.5	22.1 ± 0.1
7	10	50 ± 0.4	40 ± 0.5	87.0 ± 0.4
8	10	50 ± 0.4	10 ± 0.15	48.6 ± 0.2
9	6	50 ± 0.4	40 ± 0.5	20.7 ± 0.1
10	8	25 ± 0.2	10 ± 0.15	75.8 ± 0.3
11	6	25 ± 0.2	20 ± 0.2	88.9 ± 0.4
12	10	25 ± 0.2	20 ± 0.2	91.1 ± 0.5
13	8	25 ± 0.2	40 ± 0.5	90.2 ± 0.5
14	6	50 ± 0.4	10 ± 0.15	23.1 ± 0.1
15	8	75 ± 0.5	10 ± 0.15	14.3 ± 0.1

From the experimental design, an empirical second order polynomial equation was developed, which correlated the response and the three different process variables, as shown in Eq. 7.

$$Efficiency = 82.08 + 13.19\ pH - 28.80\ dye + 6.39\ H_2O_2 + 3.30\ pH * Dye + 8.21\ pH * H_2O_2 - 3.35\ Dye * H_2O_2 - 11.55\ pH^2 - 5.72\ Dye^2 - 26.81\ H_2O_2^2 \quad (7)$$

The correlation between the observed and predicted values is given in Figure 7. The points are placed very closely to the diagonal line indicating low discrepancies between them. Based on the aforementioned data, it can be concluded that there is a good agreement between the experimental values and the second order polynomial mathematical model, where the observed differences (i.e., the residuals) may be readily explained as random noise.

Table 7. ANOVA for the selected quadratic model

Source	df	SS	MS	F-Value	p-Value
Model	9	12330.4	1370.04	7.36	0.020
Initial pH	1	1524.66	1524.66	8.19	0.035
Dye concentration	1	7469.17	7469.17	40.14	0.001
H_2O_2 concentration	1	358.88	358.88	1.93	0.223
pH×Dye	1	56.34	56.34	0.30	0.605
pH×H_2O_2	1	327.06	327.06	1.76	0.242
H_2O_2×pH	1	57.77	57.77	0.31	0.601
pH×pH	1	361.19	361.19	1.94	0.222
Dye×Dye	1	90.75	90.75	0.49	0.516
H_2O_2×H_2O_2	1	1946.27	1946.27	10.46	0.023
Residual error	5	930.31	186.06		
Total	14	13260.71			

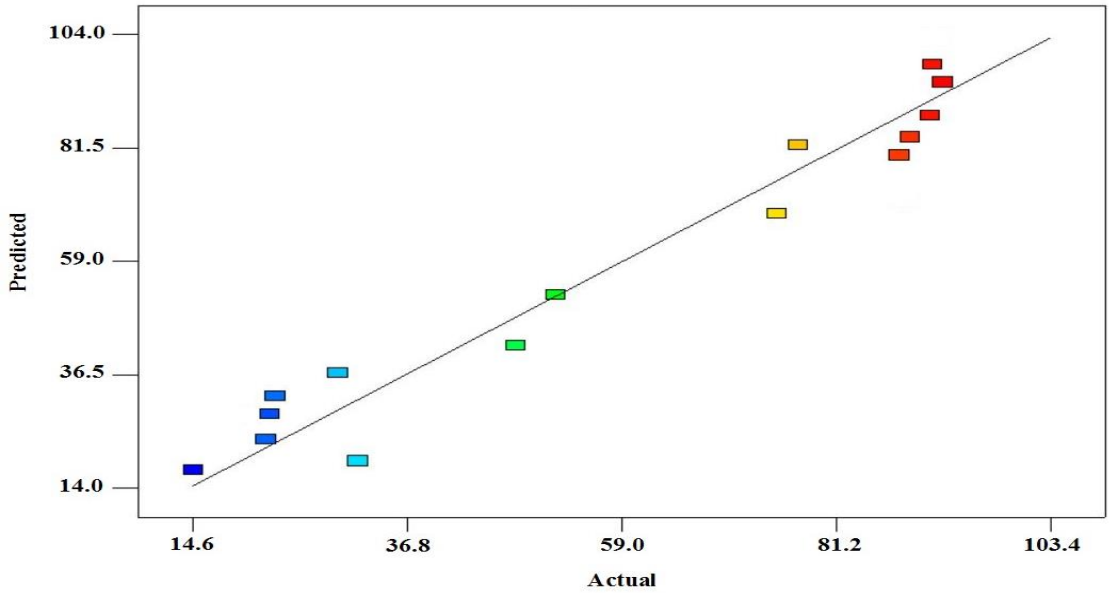

Fig. 7. Plot for correlation between the observed and predicted values

3.2.2. Effect of dye concentration, pH and H_2O_2 concentration on MB degradation efficiency

The photocatalytic reactions for MB in the solution with different dye concentrations are presented in Figure 8a. It could be seen that when the dye concentration increases, the degradation decreases. The assumed reason is that when the dye concentration increases, most of the UV irradiation will be absorbed by the dye molecules instead of H_2O_2. Therefore, generation of $^{\bullet}OH$ radicals diminish in the photodegradation of MB [23]. Figure 8b reveals that the maximum degradation takes place within the pH range of 8-10. As it can be observed, the photocatalytic activity increases with the increase in value of pH. It has been suggested that the effect of solution pH on the photocatalytic degradation is complex as this variable can modify the electrostatic interactions between the catalyst surface and substrate molecules as well as the formation of hydroxyl radicals by the reaction between hydroxide ions/H_2O and the positive holes generated in the catalyst [24,25]. The better efficiency for the degradation of MB is observed under alkaline conditions. This is due to the generation of hydroxyl radicals in the alkaline medium. In an acidic medium, degradation efficiency drops, which can be attributed due to columbic repulsion. The positively charged TiO_2 absorbs negatively charged MB, thus improving the photocatalytic degradation efficiency [26]. According to Figure 8c, the effect of H_2O_2 concentration on the degradation efficiency of MB was studied within the range of 10-40 mg/l during the photocatalytic degradation process. It shows that the increase of H_2O_2 to 20 mg/l elevates the efficiency of degradation, but if it exceeds 20 mg/l, the efficiency decreases to 38%. The first increase in H_2O_2 dosage enhanced the efficiency of degradation due to

the effect of the produced •OH radicals. But at a high dosage, H_2O_2 acts as a powerful OH scavenger. Therefore, the addition of higher values of H_2O_2 in the presence of additional hydroxyl radicals can produce hydroperoxyl radicals ($^{\bullet}HO_2$), which are much less reactive and do not contribute to the oxidative degradation of organic compounds [11].

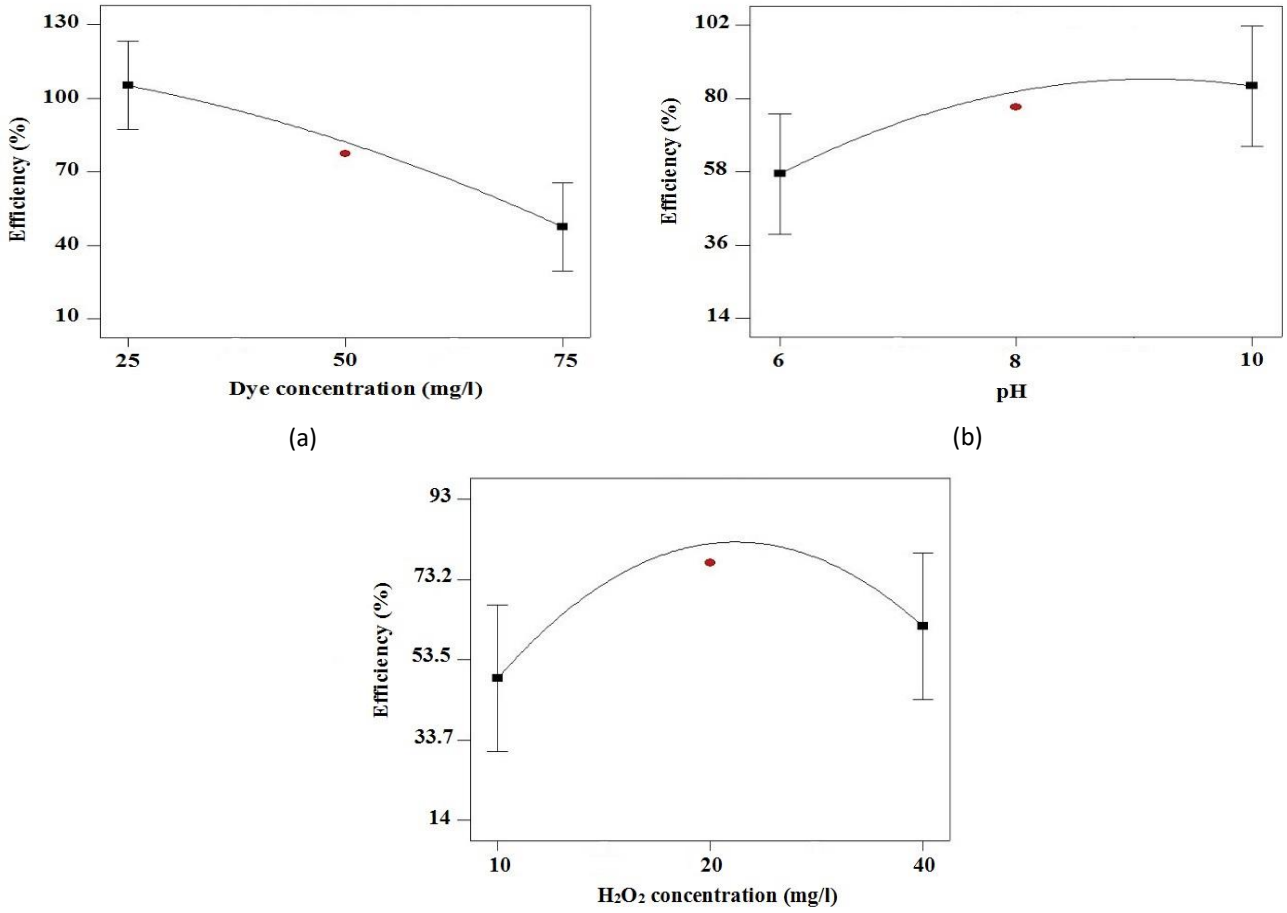

Fig. 8. Diagram for (a) dye concentration, (b) pH, and (c) H_2O_2 concentration versus MB degradation efficiency

Figure 9 indicates the efficiency of MB degradation at different pH levels and different H_2O_2 concentrations. It shows that the highest efficiency occurs when pH is more than 8 and the concentration of H_2O_2 is within the range of 20-30 mg/l. The efficiency of dye degradation with initial pH and different dye concentrations has been demonstrated in Figure. 10. According to this figure, the highest efficiency occurs within the pH range of 8.5-9.5 and when the dye concentration is low.

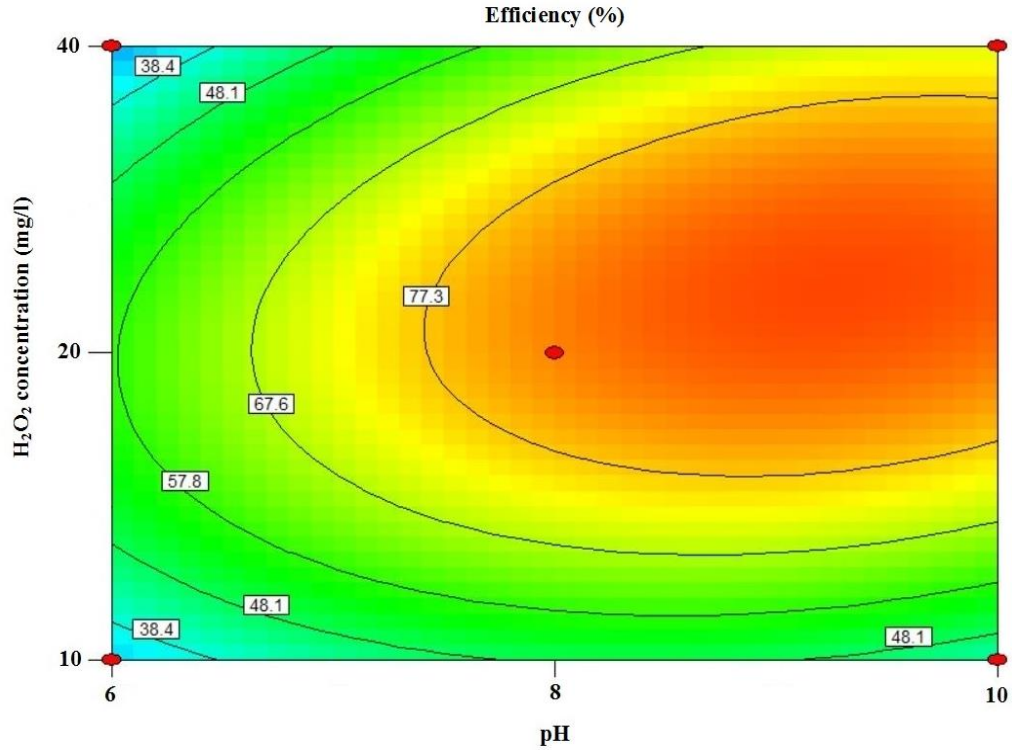

Fig. 9. Contour plot of MB degradation efficiency versus initial pH and H_2O_2 concentration

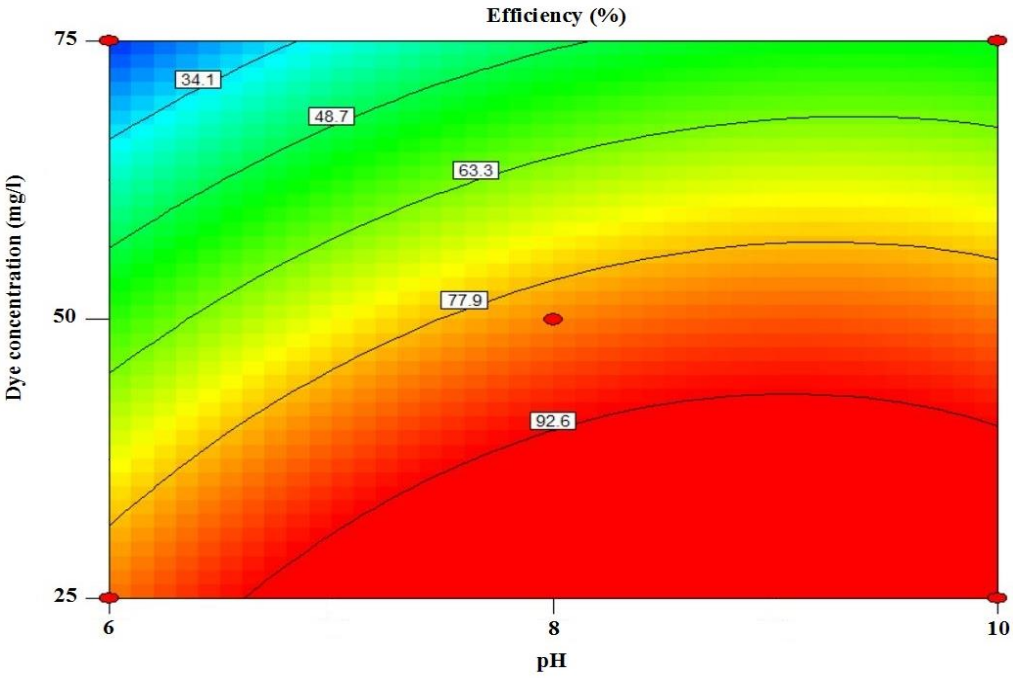

Fig. 10. Contour plot of MB degradation efficiency versus initial pH and dye concentration

4. Conclusions

The results of this research indicated that Fe^{3+} doped TiO_2 supported on natural zeolite can be used as a practical method for degrading MB from textile wastewaters. The experiments were modeled and optimized by RSM with ANOVA Table, indicating that the dye concentration and pH are the most effective factors in these experiments. The optimization results revealed that the maximum percentage of degradation was achieved at the dye concentration of 25 mg/L, initial pH of 10, and H_2O_2 concentration of 40 mg/L, with the efficiency under these conditions reaching 92% with a 90 min retention time and 1 g/L catalyst concentration.

Acknowledgement

The authors greatly acknowledge the Gol Nesar Textile Company for supplying the dye. We also appreciate the support of the Environmental Research Institute and Central Laboratory of the University of Isfahan.

References

[1] Alimohammadi, Z., Younessi, H., Bahramifar, N. (2016). Desorption reactive red 198 from activated carbon prepared from walnut shells: Effects of temperature, sodium carbonate concentration and organic solvent dose. *Environmental science* and *technology*, *3*, 137-141.

[2] Yang, Y., Xu, L., Wang, H., Wang, W., Zhang, L. (2016). TiO_2/graphene porous composite and its photocatalytic degradation of methylene blue. *Materials and design*, *108*, 632-639.

[3] Bhuyan, B., Paul, B., Dhar, S. S., Vadivel, S. (2017). Facile hydrothermal synthesis of ultrasmall W18O49 nanoparticles and studies of their photocatalytic activity towards degradation of methylene blue. *Materials chemistry and physics*, *188*, 1-7.

[4] Asl, M. I., Ghazi, M. M., Jahangiri, M. (2016). Synthesis, characterization and degradation activity of Methyl orange Azo dye using synthesized CuO/α-Fe_2O_3 nanocomposite, *Advances in Environmental Technology,* 2(3), 143-151.

[5] Dariani, R. S., Esmaeili, A., Mortezaali, A., Dehghanpour, S. (2016). Photocatalytic reaction and degradation of methylene blue on TiO_2 nano-sized particles. *Optik-international journal for light and electron optics*, *127*(18), 7143-7154.

[6] Bian, X., Hong, K., Liu, L., Xu, M. (2013). Magnetically separable hybrid CdS-TiO2-Fe_3O_4 nanomaterial: Enhanced photocatalystic activity under UV and visible irradiation. *Applied sSurface science*, *280*, 349-353

[7] Asvadi, F., Fallah, N., Elyasi, S., Mohseni, F. (2017). Investigation of affecting operational parameters in photocatalytic degradation of reactive red 198 with TiO_2: optimization through response surface methodology, *Advances in Environmental Technology,* 2(4) 169-177.

[8] Arimi, A., Farhadian, M., Solaimany Nazar, A.R., Homayoonfal, M. (2016). Assessment of operating parameters for photocatalytic degradation of a textile dye by Fe_2O_3/TiO_2/clinoptilolite nanocatalyst using Taguchi experimental design. *Research on Chemical Intermediates, 42*, 4021-4040.

[9] Liu, H., Shon, H. K., Sun, X., Vigneswaran, S., Nan, H. (2011). Preparation and characterization of visible light responsive Fe_2O_3–TiO_2 composites. *Applied surface science*, *257*(13), 5813-5819.

[10] Yao, K., Basnet, P., Sessions, H., Larsen, G. K., Murph, S. E. H., Zhao, Y. (2016). Fe_2O_3–TiO_2 core–shell nanorod arrays for visible light photocatalytic applications. *Catalysis today*, *270*, 51-58.

[11] Niu, P., Hao, J. (2013). Photocatalytic degradation of methyl orange by titanium dioxide-decatungstate nanocomposite films supported on glass slides. *Colloids and Surfaces A: Physicochemical and engineering aspects*, *431*, 127-132.

[12] Song, J., Xu, Z., Liu, W., Chang, C. T. (2016). $KBrO_3$ and graphene as double and enhanced collaborative catalysts for the photocatalytic degradation of amoxicillin by UVA/TiO_2 nanotube processes. *Materials science in semiconductor processing*, *52*, 32-37.

[13] Zheng, R., Zhang, H., Liu, Y., Wang, X., Han, Z. (2017). Ag-ligand modified tungstovandates and their efficient catalysis degradation properties for methylene blue. *Journal of solid state chemistry*, *246*, 258-263.

[14] Liu, F., Jamal, R., Wang, Y., Wang, M., Yang, L., Abdiryim, T. (2017). Photodegradation of methylene blue by photocatalyst of DAD type polymer/functionalized multi-walled carbon nanotubes composite under visible-light irradiation. *Chemosphere*, *168*, 1669-1676.

[15] Park, J. H., Jang, I., Song, K., Oh, S. G. (2013). Surfactants-assisted preparation of TiO2–Mn oxide composites and their catalytic activities for degradation of organic pollutant. *Journal of physics and chemistry of solids*, *74*(7), 1056-1062

[16] Amini, M., Pourbadiei, B., Ruberu, T. P. A., Woo, L. K. (2014). Catalytic activity of MnO x/WO_3 nanoparticles: synthesis, structure characterization and oxidative degradation of methylene blue. *New journal of chemistry*, *38*(3), 1250-1255.

[17] Zhang, L., Nie, Y., Hu, C., Hu, X. (2011). Decolorization of methylene blue in layered manganese oxide suspension with H_2O_2. *Journal of hazardous materials*, *190*(1-3), 780-785.

[18] Mehrabian, M., Esteki, Z. (2017). Degradation of methylene blue by photocatalysis of copper assisted ZnS nanoparticle thin films. *Optik-international journal for light and electron optics*, *130*, 1168-1172.

[19] Wang, C., Shi, H., Li, Y. (2011). Synthesis and characteristics of natural zeolite supported Fe^{3+}-TiO_2 photocatalysts. *Applied surface science*, *257*(15), 6873-6877.

[20] Korkuna, O., Leboda, R., Skubiszewska-Zie, J., Vrublevs'ka, T., Gun'ko, V. M., Ryczkowski, J. (2006). Structural and physicochemical properties of natural zeolites: clinoptilolite and mordenite. *Microporous and mesoporous materials*, *87*(3), 243-254.

[21] Battisha, I. K., Afify, H. H., Ibrahim, M. (2006). Synthesis of Fe_2O_3 concentrations and sintering temperature on FTIR and magnetic susceptibility measured from 4 to 300 K of monolith silica gel prepared by sol–gel technique. *Journal of magnetism and magnetic materials*, *306*(2), 211-217.

[22] Kannaiyan, D., Kochuveedu, S. T., Jang, Y. H., Jang, Y. J., Lee, J. Y., Lee, J., Kim, D. H. (2010). Enhanced photophysical properties of nanopatterned titania nanodots/nanowires upon hybridization with silica via block copolymer templated sol-gel process. *Polymers*, *2*(4), 490-504.

[23] Sohrabi, M. R., Khavaran, A., Shariati, S., Shariati, S. (2017). Removal of Carmoisine edible dye by Fenton and photo Fenton processes using Taguchi orthogonal array design. *Arabian journal of chemistry*, *10*, S3523-S3531

[24] Nadarajan, R., Bakar, W. A. W. A., Ali, R., Ismail, R. (2016). Photocatalytic degradation of 1, 2-dichlorobenzene using immobilized $TiO_2/SnO_2/WO_3$ photocatalyst under visible light: application of response surface methodology. *Arabian journal of chemistry*, 11(1), 34-47.

[25] Lambropoulou, D., Evgenidou, E., Saliverou, V., Kosma, C., & Konstantinou, I. (2017). Degradation of venlafaxine using TiO2/UV process: kinetic studies, RSM optimization, identification of transformation products and toxicity evaluation. *Journal of hazardous materials*, *323*, 513-526.

[26] Devadi, M. A. H., Krishna, M., Murthy, H. N., & Sathyanarayana, B. S. (2014). Statistical optimization for photocatalytic degradation of methylene blue by Ag-TiO_2 nanoparticles. *Procedia materials science*, *5*, 612-621.